Carrier transport through grain boundaries in semiconductors

G. Blatter and F. Greuter
Brown Boveri Research Center, CH-5405 Baden, Switzerland
(Received 30 September 1985)

The transport of majority carriers through an electrically active grain boundary is treated for the situation where deep traps are an essential feature of the bulk semiconductor. Electrons trapped at the interface are screened by the ionized defect states within the depletion regions and thereby a double Schottky potential barrier is formed. The leakage and nonlinearity of the steady-state current across such a grain boundary depend strongly on the distribution of interface states and on the density of the available screening charge. The ac small-signal conductance and capacitance are governed by both the finite response time of the interface and the deep bulk traps. From measurements of the static and dynamic quantities it is then possible to determine the microscopic parameters of the grain boundary.

I. INTRODUCTION

The physics of grain boundaries in polycrystalline semiconductors has attracted increasing interest over the past few years.[1] Progress has been made in understanding some of the fundamental aspects of grain boundaries such as their atomic[2] and electronic[1,3] structure or the grain-boundary total energy.[3] An important field of interest is the transport properties of these materials, which are usually dominated by the formation of potential barriers at the grain boundaries. Many technical applications[1] rely on such grain-boundary phenomena (ZnO varistors, boundary-layer capacitors) or at least have to deal with them (polycrystalline Si devices, solar cells). Any improvement of such devices is therefore based on a thorough knowledge of the underlying physical phenomena.

The electrical properties of grain boundaries have thus been extensively studied experimentally as well as theoretically.[4–13] On the experimental side the admittance spectroscopy[5,7,11–13] has proved to be a very useful tool for the study of the microscopic grain-boundary parameters. These measurements can provide information on the density of interface states, their trapping cross section, and the relaxation time. The corresponding quantities can as well be determined for the donor and acceptor states in the depletion regions adjacent to the interface. Equivalent information can be gained by the well-known technique of deep-level transient spectroscopy[14] (DLTS) as the underlying physics is basically the same.

In this paper we give a self-consistent description of the static and dynamic properties of carrier transport over a double Schottky barrier forming at a grain boundary. A finite density of states within the gap is responsible for the charging of the interface. For the first time the screening charge for the interface is assumed to include an arbitrary number of deep bulk donor (acceptor) levels besides the shallow defects. Two extreme models are discussed for the relaxation properties of the grain boundary. The first considers strongly localized interface traps such that the quasiequilibrium is established only with the bulk. The second treats perfect relaxation within the interface itself. The physical situation, in general, then will be somewhere between these two limits.

Models for the admittance of grain boundaries have been developed by Seager and Pike[7,12] and by Werner;[11] however, the role of the deep bulk traps is not included in their analysis. On the other hand, several model calculations for p-n junctions or Schottky contacts in the presence of deep volume traps have been reported in the literature.[15–17]

Here we will show that deep traps can have a strong effect on the *static* and *dynamic* properties of carrier transport through a grain boundary. Their presence contributes to the screening of the interface charge and thereby to a destabilization of the static barrier. Dynamically, the deep traps lead to a dispersion in the small-signal admittance even at zero bias. Such a dispersion, which can change the zero-bias conductance by several orders of magnitude, has been found in polycrystalline ZnO (varistors).[5,18,19]

The modifications of the carrier transport due to the interface states can be well separated from those generated by the deep traps. Whereas the former have a strong influence on the small-signal capacitance at low bias, the latter are best studied by analyzing the small-signal conductance. The comparison of experiments with the present model calculations then allows for the determination of the microscopic parameters of the interface and the deep trap states.

The outline of the paper is as follows. In Sec. II we describe the steady-state properties of a grain-boundary barrier in the presence of an arbitrary number of deep bulk traps. The time-dependent properties of the carrier transport without the influence of deep levels are briefly reviewed in Sec. III, where we also present a short discussion of the interface relaxation properties. The full dynamic behavior including deep trap effects is then developed in Sec. IV. In Sec. V we summarize our results.

The theory presented in this paper describes the transport of *majority* carriers through a grain boundary. In the high-field regime new phenomena are observed which can be attributed to *minority* carrier generation by hot electrons in the depletion region.[19] First there is a strong destabilization of the barrier at large bias, leading to an electrical breakdown with nonlinearity coefficients $\alpha = d(\log j)/d(\log V)$ as large as $\alpha \sim 200$. A second effect shows up in the small-signal capacitance which becomes negative at large bias. Most directly the presence of the minority carriers is observed in recombination luminescence experiments.[20,21] A model for their inclusion in the description of the transport properties has recently been proposed by Pike,[19] but a detailed analysis has not been published. The full model treating deep trap effects and minority carriers is the topic of a second publication on carrier transport through grain boundaries. The comparison of these theoretical calculations with experiments on polycrystalline ZnO will then be the final paper in this series.

II. STEADY STATE

A grain boundary in a semiconductor becomes electrically active as a result of charge trapping by gap states localized between two adjacent grains. Such interface states are possibly created by dislocations introduced by the crystallographic mismatch between the adjacents grains, thereby leading to dangling bonds or other interfacial defects. A second possible origin of these states are dopant or impurity atoms trapped at the interface and acting as donor or acceptor levels. The diffusion of these atoms into the bulk of the grains is strongly suppressed in this case, e.g., by size misfit. The width of such an interfacial region typically amounts to ~ 10 Å.[22] The idealization of an infinitely thin interface in our model is therefore well justified.

The electric field generated by the charged interface gives rise to a band bending in the adjacent grains. The depletion of majority carriers leads to the buildup of a screening charge due to ionized shallow defects. Additional screening charge is provided by deep bulk gap states. These charged centers may be intrinsic (defects) or are introduced by controlled doping.

The geometry of the energy bands around a plane charged interface is easily calculated in the Schottky approximation. The Poisson equation

$$\frac{d^2}{dx^2}\Phi(x) = \frac{\rho(x)}{\epsilon_0 \epsilon} \quad (1)$$

for the potential $\Phi(x)$ has to be solved for a charge distribution $\rho(x)$ of the form (see Fig. 1)

$$\rho(x) = e\sum_{\nu=0}^{n} N_\nu[\Theta(x + x_{l\nu}) - \Theta(x - x_{r\nu})] - Q_i\delta(x) .$$

The reduction to a one-dimensional problem is due to the translational invariance of the plane interface. The interface charge is denoted by Q_i, the trap densities by N_ν, the dielectric constant is ϵ, ϵ_0 is the permittivity of the vacuum, and e the unit charge. In (1) we adopt the convention $e = |e|$ such that the potential energy of an electron is simply $e\Phi(x)$. Finally, $\Theta(x)$ and $\delta(x)$ are the Heaviside step function and the Dirac δ function, respectively.

Here we restrict the discussion to donor states in an n-type semiconductor. The extension to deep acceptor levels or p-type material is straightforward.[23(a)] N_0 is the density of the shallow donor which is often the dominating trap and which we assume to be ionized everywhere.

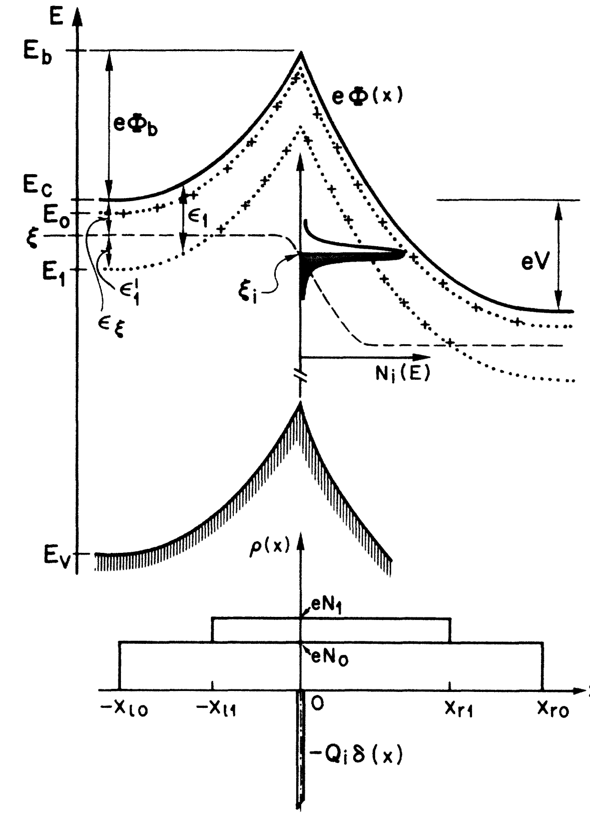

FIG. 1. Energy-band diagram and charge distribution for a double Schottky barrier forming at a grain boundary. For the sake of clarity only one deep bulk trap level is included.

The solution of Eq. (1), subject to the boundary conditions

$$\Phi(-\infty) = \Phi(-x_{l0}) = 0 \quad \text{and} \quad \Phi(\infty) = \Phi(x_{r0}) = -V ,$$

is given by

$$\Phi(x) = \begin{cases} \sum_{\nu=0}^{\mu} \frac{\gamma_\nu}{2}(x + x_{l\nu})^2, & -x_{l,\mu} \le x \le -x_{l,\mu+1} \\ \sum_{\nu=0}^{\mu} \frac{\gamma_\nu}{2}(x - x_{r\nu})^2 - V, & x_{r,\mu+1} \le x \le x_{r,\mu} . \end{cases} \quad (2)$$

For $\mu = n$ we define $x_{l,n+1} = x_{r,n+1} = 0$. Here V is the bias applied across the grain boundary (see Fig. 1) and

$$\gamma_\nu = \frac{eN_\nu}{\epsilon_0\epsilon}, \quad \gamma = \sum_{\nu=0}^{n} \gamma_\nu .$$

The positions $x_{l\nu}$ and $x_{r\nu}$ are determined by the conditions

$$\Phi(0^-) = \Phi(0^+) = \Phi_b , \quad (3)$$

$$\Phi'(0^-) - \Phi'(0^+) = Q_i/\epsilon_0\epsilon , \quad (4)$$

and

$$e\Phi(-x_{l\nu})=e\Phi(x_{r\nu})+eV=\epsilon_\nu-\epsilon_\xi=\epsilon'_\nu,\quad \nu\geq 1\ . \tag{5}$$

The new symbols introduced above are Φ_b for the barrier height and $\epsilon_\nu, \epsilon_\xi$ for the positions of the deep traps and the bulk Fermi level relative to the conduction band (Fig. 1).

The above $2n+3$ conditions have to be solved for the $2(n+1)$ positions $x_{l\nu}$ and $x_{r\nu}$, $\nu=0,\ldots,n$, and the *barrier height* Φ_b. This calculation is rather tedious and the derivation is given in the Appendix. The result is

$$x_{l0}=\left[\frac{V_c}{2\gamma}\right]^{1/2}\left[1-\frac{V}{V_c}\right]+\alpha_n,\quad V_c=\frac{1}{2\gamma}\left[\frac{Q_i}{\epsilon_0\epsilon}\right]^2$$

$$x_{l\nu}=x_{l0}-(b_\nu)^{1/2},\quad \nu\geq 1$$

$$x_{r\nu}=x_{l\nu}+\left[\frac{2}{\gamma V_c}\right]^{1/2}V,\quad \nu\geq 0$$

with the b_ν defined recursively by

$$(b_\nu)^{1/2}=\alpha_{\nu-1}+\left[n_0^{\nu-1}\left[a_\nu-\sum_{\mu=1}^{\nu-1}n_\mu^{\nu-1}a_\mu\right]\right]^{1/2},\quad \nu\geq 2$$

$$\alpha_\nu=\sum_{\mu=1}^{\nu}n_\mu^\nu(b_\mu)^{1/2},\quad a_\nu=\frac{2}{e\gamma_0}\epsilon'_\nu$$

and the starting value

$$b_1=n_0^0a_1=\frac{2}{e\gamma_0}\epsilon'_1\ .$$

The constants n_μ^ν are the relative weights for the deep traps,

$$n_\mu^\nu=\frac{N_\mu}{\sum_{\lambda=0}^{\nu}N_\lambda}\ .$$

Despite this complicated result for the boundaries of the deep trap screening charges, $x_{l\nu}$ and $x_{r\nu}$, the result for the barrier height Φ_b turns out to be very simple (see the Appendix)

$$\Phi_b=\tfrac{1}{4}V_c\left[1-\frac{V}{V_c}\right]^2+\frac{1}{e\gamma}\sum_{\nu=1}^{n}\gamma_\nu\epsilon'_\nu,\quad V\leq V_c\ . \tag{6}$$

When a bias V is applied to the junction, the barrier Φ_b is lowered by a reduction of the first term in Eq. (6). The second term in (6) initially is voltage independent. However, as V is increased, an ionized deep trap, say $\nu=\lambda$, disappears below the quasi-Fermi-level and is neutralized completely as soon as $e\Phi_b<\epsilon'_\lambda$.[24]

As

$$\frac{1}{\gamma}\sum_{\nu=1}^{\lambda}\gamma_\nu\epsilon'_\nu<\frac{1}{\gamma}\sum_{\nu=1}^{\lambda}\gamma_\nu\epsilon'_\lambda=\epsilon'_\lambda$$

(the traps $\nu>\lambda$ have already disappeared) it follows from (6) that the condition $e\Phi_b(V)<\epsilon'_\lambda$ for the neutralization of the trap λ is reached at a bias $V<V_c$. Therefore the second term in (6) also disappears as $V\to V_c$ and hence $\Phi_b\to 0$ as $V\to V_c$.

The remaining free parameter in the geometry of the barrier is the voltage-dependent *interface charge* Q_i. This is determined by the interface density of states (DOS) $N_i(E)$ which is fixed with respect to the valence band. The electron traps are filled up to the (quasi-) Fermi level ξ_i of the interface,

$$Q_i=e\int_{\xi_i^n}^{\infty}dE\,N_i(E)f_i(E)\ , \tag{7}$$

with

$$f_i(E)=\frac{1}{1+e^{(E-\xi_i)/k_BT}}\ .$$

The integration in Eq. (7) proceeds from the Fermi level ξ_i^n of the neutral interface.[6,23(b)] This allows for the filling of some traps in the lower part of the band gap without generating any net charge at the interface.

For zero-bias conditions the Fermi level is constant throughout the bicrystal, i.e., $\xi_i(V=0)=\xi$, whereas for $V>0$ the quasi-Fermi-level at the interface is shifted with respect to the bulk Fermi level[25(a),25(b)]

$$\Delta\xi=\xi-\xi_i=k_BT\ln\frac{2}{1+e^{-eV/k_BT}}\ .$$

The above shift is determined by the detailed balance condition for the interface, i.e., the number of electrons trapped and emitted by the interface have to be equal.

As mentioned above, the interface density of states $N_i(E)$ is fixed with respect to the valence band at $x=0$. Therefore $N_i(E)$ shifts with respect to ξ_i as the barrier height Φ_b is changed. This results in a dependence of the interface charge Q_i on the barrier height Φ_b [Eq. (7)]. Thus as we apply a bias V to the junction, the barrier is reduced as is clear from Eq. (6); on the other hand, the reduction is partly compensated by an increase of the trapped charge Q_i as long as $N_i(\xi_i)$ is finite. Hence, with increasing bias more charge is filled into the interface and the barrier is stabilized. Only when $N_i(\xi_i)\to 0$, i.e., all interface states are filled, can the barrier decay rapidly as given by (6) for a constant Q_i. The (local) stabilization of Φ_b is stronger for a larger $N_i(\xi_i(V))$.

This is illustrated in Fig. 2 where the bias dependence of the barrier height Φ_b and the charge Q_i (calculated self-consistently) are shown. Examples are given for a *single interface level* $[N_i(E)=N_i\delta(E-E_i)]$, a *Gaussian density of states* (centered at E_i with variance ΔE and integrated density N_i), and a *rectangular shape* (centered at E_i with half width ΔE and total density N_i). The numerical values for the parameters are listed in Table I. No traps are taken into account yet.

In all cases there is an obvious collapse of the barrier height as soon as all interface states are filled. The barrier is strongly pinned for the sharply peaked DOS. The influence of the deep trap states on the barrier height Φ_b is illustrated in Fig. 3. An increase in the deep trap density always decreases the first term in Eq. (6) but increases the second. However, it is easy to show that the net effect is a decrease[26] in the barrier height because

$$\frac{\partial\Phi_b}{\partial N_\lambda}<\frac{1}{\epsilon_0\epsilon\gamma}(\epsilon'_\lambda-e\Phi_b)<0\ .$$

The last inequality is the ionization condition for the trap λ as discussed above. Figure 3 shows that the barrier

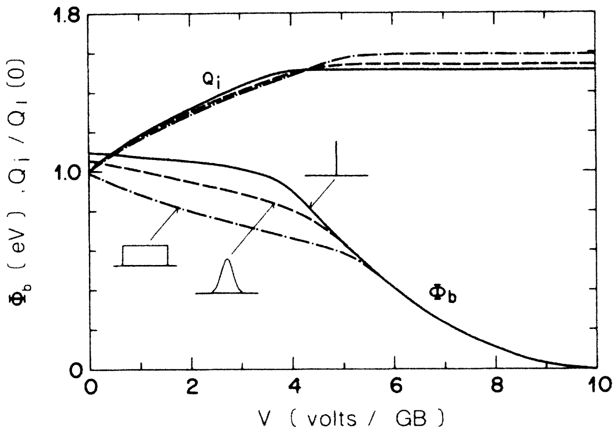

FIG. 2. Barrier height Φ_b and interface charge Q_i versus applied bias V. We compare the stability of Φ_b for a single level, a Gaussian, and a rectangular DOS for the interface. The values for the parameters and the zero-bias interface charge $Q_i(0)$ are listed in Table I. No bulk traps are included here. GB denotes grain boundary.

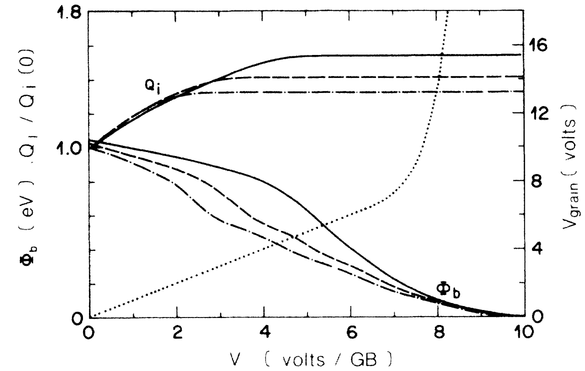

FIG. 3. Barrier height $\Phi_b(V)$ and interface charge $Q_i(V)$ for a Gaussian DOS for the interface. The situation with no traps (——) is compared to the cases of a moderate [— — —, case (a) in Table I] and a large [—·—·—·, case (b) in Table I] density of deep bulk defects. Also shown is the relationship between the total bias drop across the grain V_{grain} and the grain-boundary bias V (· · · ·). There is only a minor dependence of V_{grain} on the trap density and the interface DOS.

height $\Phi_b(V)$ is strongly affected by the deep traps: (i) the interface charge $Q_i(0)$ is larger (Table I); (ii) the interface is filled faster and thus the barrier decays earlier, and (iii) the neutralization of a deep trap at $e\Phi_b \sim \epsilon'_\lambda$ leads to a local stabilization.

At large applied bias where Φ_b is small, the finite conductivity of the grains has to be taken into account. The voltage drop across a single grain is then divided up into a bulk part and a contribution from the grain boundary. The equality of the current following through the bulk and over the barrier into the next grain determines the ratio of the two voltages. We show the result of such a (self-consistent) calculation in Fig. 3 where the total bias across a single grain is plotted versus the bias drop at the grain boundary. There is a sharp separation between the barrier-dominated conductivity at low bias and the bulk-dominated part at large bias.

We conclude this section with a discussion of the *carrier transport* through the grain boundary within the thermionic emission model.

The electron current emitted over the barrier Φ_b into the positively biased grain is

$$A^* T^2 e^{-(e\Phi_b + \epsilon_\xi)/k_B T} ,$$

with A^* the Richardson constant, T the temperature, and

TABLE I. List of microscopic parameters for the grain boundaries described in Figs. 2—9. (The temperature is 400 K, the energy gap is 3.2 eV, the dielectric constant is 9, the effective mass is 0.25, the grain size is 15 μm, the grain conductivity is 10.8 S cm^{-1}, the Richardson constant is 30 A cm^{-2} K^{-2}, and the Fermi level ϵ_ξ equals 0.067 eV.)

Interface	E_i[a] (eV)	ΔE (eV)	N_i (cm^{-2})	c (cm^2)	$Q_i(0)$ ($10^{12}e$)		
(single level)	2.0		10^{13}	10^{-13}	6.64		
(Gaussian)	2.0	0.15	10^{13}	10^{-13}	6.52	case (a): 7.09	case (b): 7.57
(rectangular)	2.0	0.5	10^{13}	10^{-13}	6.31		

Bulk traps	ϵ_v (eV)	N_v (cm^{-3}) case (a)	N_v (cm^{-3}) case (b)	c_v (cm^2)	τ_v (s)	ω_{res} (s^{-1})
Shallow	0.02	10^{18}	10^{18}	10^{-14}	0	∞
Deep	0.2	5×10^{16}	10^{17}	10^{-14}	7.36×10^{-10}	1.36×10^{9}
Deep	0.4	10^{17}	2×10^{17}	10^{-14}	2.44×10^{-7}	4.10×10^{6}
Deep	0.6	2×10^{17}	4×10^{17}	10^{-14}	8.07×10^{-5}	1.24×10^{4}

[a] E_i is measured with respect to the valence-band edge at $x=0$.

k_B the Boltzmann constant. A second current, suppressed by the factor $\exp(-eV/k_BT)$, is flowing in the opposite direction. These are the two main currents at the junction. A fraction of these currents is trapped and reemitted by the interface states. The trapping is asymmetric for $V>0$,

$$j_t = j_{tl} + j_{tr} = j(1+e^{-eV/k_BT}) \int dE\, c(E) N_i(E)[1-f_i(E)] \,, \tag{8}$$

with

$$j = A^* T^2 e^{-(e\Phi_b+\epsilon_\xi)/k_BT} \,,$$

whereas the emitted current is distributed symmetrically,

$$j_{\rm em} = \int dE\, b(E) e^{-(E_b-E)/k_BT} N_i(E) f_i(E) \,. \tag{9}$$

The capture cross section $c(E)$ and the charge emission rate $b(E)$ are approximated by constants and can be related to one another by the detailed balance condition[25(a)] ($b=2Ac$, $A=A^*T^2$). The energy E_b corresponds to the top of the barrier (see Fig. 1).

The two currents j_t and $j_{\rm em}$ are responsible for the updating of the interface charge Q_i whenever the external bias V is changed. Therefore they control the main currents flowing over the barrier. Their importance will become clearer when the time-dependent properties are discussed in the next section.

The external dc current flowing through the grain boundary finally is the weighted sum of the above currents, which can be evaluated on either side of the interface. From now on we choose the left side in our discussion. We then find

$$j_{\rm dc} = j_{lb} = j(1-e^{-eV/k_BT}) - \tfrac{1}{2} j_{\rm em} + j_{rt} \tag{10}$$

$$= j(1-\hat{c}/2)(1-e^{-eV/k_BT}) \,, \tag{11}$$

with the total capture probability

$$\hat{c} = c \int dE\, N_i(E)[1-f_i(E)] \,. \tag{12}$$

The factor $1-\hat{c}/2$ is due to the asymmetry in capture and emission.

The external current $j_{\rm dc}$ contains the exponential of the barrier height $e\Phi_b$ in units of k_BT. Typical values of $e\Phi_b$ are on the scale of 1 eV. Therefore the current strongly depends on every detail of the function $\Phi_b(V)$. This is illustrated in Fig. 4 where we show the large variations in dc current as the bias V is changed. For comparison different densities are considered for the interface states (single level, Gaussian, broad rectangular) and for the deep traps. At low bias ($eV \ll k_BT$) the j-V characteristic is *Ohmic* as Φ_b is constant on this energy scale. At higher voltages the factor $1-\exp(-eV/k_BT)$ in Eq. (10) tends towards a saturation. This competes with the exponential rise of the current when the barrier Φ_b decays. For a stable barrier *sub-Ohmic* behavior can be seen in this region. As the interface is filled the barrier collapses and the current rises by several orders of magnitude. This is called the *breakdown regime.* Finally, at very large bias, a *second Ohmic regime* is entered when the current limiting process is given by the finite conductivity of the grains (see also Fig. 3).

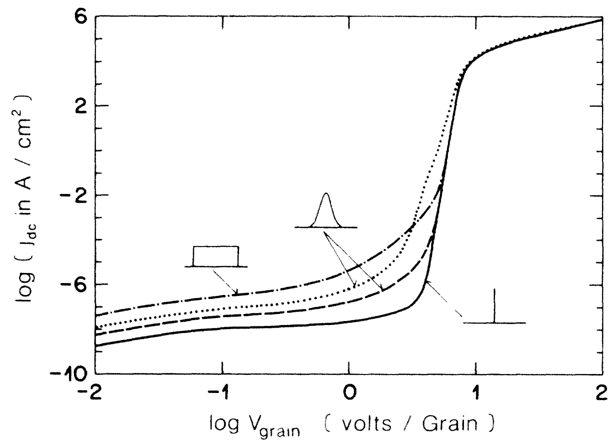

FIG. 4. dc current $j_{\rm dc}$ versus applied bias $V_{\rm grain}$. A single-level DOS for the interface (no deep traps) leads to the highest nonlinearity with a pronounced saturation regime. This is compared to a Gaussian (— — —) and a rectangular DOS without deep traps and the same Gaussian DOS when deep bulk defects [· · · ·, case (a) in Table I] are present.

Usually the breakdown behavior is quantified by the *nonlinearity coefficient* $\alpha = d(\log j)/d(\log V)$, which is shown in Fig. 5 for the data of Fig. 4. High values for α are obtained when the interface is rapidly filled at a large bias V. For reasonable parameters, α can be as high as ~ 40. The dips in $\alpha(V)$, for the case including deep bulk traps, indicate the local stabilization of the barrier when the screening charge is reduced with the disappearance of a deep trap level (see also Fig. 3).

The lowering of the deep trap density leads to a reduction in leakage and to a larger nonlinearity α as is evident from Figs. 4 and 5.

The thermionic emission model for the currents applies

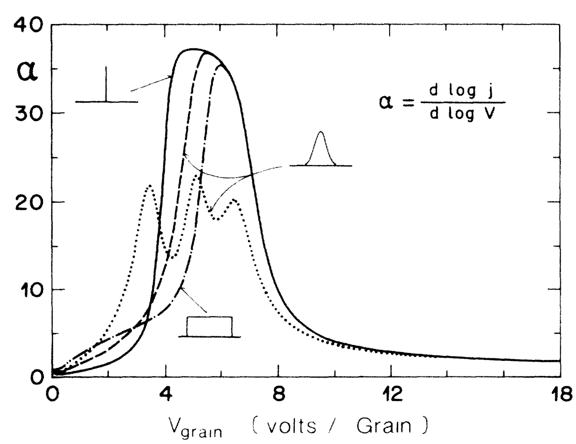

FIG. 5. Nonlinearity parameter α versus applied total bias $V_{\rm grain}$ for the grain-boundary models of Fig. 4.

sufficiently well to a large variety of materials, including polycrystalline Si,[7,11] GaAs,[7,8] and ZnO.[13] For highly doped samples and at low temperatures, however, phonon-assisted tunneling[7,27] cannot be neglected.

III. TIME-DEPENDENT PROPERTIES WITHOUT DEEP BULK TRAPS

In this section we calculate the time-dependent properties of carrier transport through a grain boundary in linear response. The effects from deep bulk traps are not yet taken into account. Three models for the interface are discussed: The simplest case of a single interface level is examined in Sec. III A. In Secs. III B and III C the modifications due to a continuous density of states are discussed. The case of strongly localized states is presented in Sec. III B, whereas Sec. III C deals with the case of perfect relaxation within the interface itself. No such differentiation has to be made for the single level.

A. Single interface level

When a time-dependent bias

$$V(t)=V_0+\tilde{V}e^{i\omega t}, \quad e\tilde{V}\ll k_B T \tag{13}$$

is applied across the grain boundary the interface charge Q_i as well as the screening charge from the ionized shallow donor become time dependent. One consequence of the resulting change in the barrier geometry is a modulation of the main currents emitted over the barrier.[7] This modulation is delayed in time with respect to the applied bias $V(t)$ since any change in interface charge Q_i involves trapping (j_t) and emission (j_{em}) processes which are not instantaneous. The exponential amplification of the variation of the barrier Φ_b [and by Eq. (7) of Q_i] in the external current can then be used to study the dynamics of the interface.

A second effect is caused by the time dependence of the shallow donor screening charge which leads to a displacement current. This is again shifted in phase with respect to $V(t)$ and gives a second contribution to the small-signal capacitance of the grain boundary.

We first study the *dynamics of the interface charge* Q_i. The net current flowing into the interface is given by the difference

$$j_i=j_t-j_{\mathrm{em}}=\tilde{j}_i e^{i\omega t} .$$

Expanding Eqs. (8) and (9), we find for the linear response $\tilde{j}_i$ the expression

$$\tilde{j}_i=j_0\frac{e\hat{c}_0}{k_B T}(1+e^{-eV_0/k_B T}) \times\left[\left[\tilde{\Phi}_b-\frac{\tilde{V}}{1+e^{eV_0/k_B T}}\right]-\frac{k_B T}{e}\frac{\tilde{f}_i}{f_{i0}(1-f_{i0})}\right] ,$$

where we have used similar expressions as Eq. (13) for the time dependence of the barrier height $\Phi_b=\Phi_{b0}-\tilde{\Phi}_b\exp(i\omega t)$ and the interface occupation $f_i=f_{i0}+\tilde{f}_i\exp(i\omega t)$.[28] The single interface level is described by the density of states $N_i(E)=N_i\delta(E-E_i)$. The constants $\hat{c}_0=cN_i(1-f_{i0})$ and $j_0=A\exp[-(e\Phi_{b0}+\epsilon_\xi)/k_B T]$ are the steady-state parts of the capture probability $\hat{c}$ and the current j, respectively.

The finite interface current j_i limits the rate of change of the charge Q_i. Integrating the equation of continuity,

$$j_i=\frac{dQ_i}{dt}=i\omega\tilde{Q}_i e^{i\omega t} ,$$

leads to the result

$$\tilde{Q}_i=C_i(\omega)\left[\tilde{\Phi}_b-\frac{\tilde{V}}{1+e^{eV_0/k_B T}}\right] , \tag{14}$$

with the interface capacitance $C_i(\omega)$ given by

$$C_i(\omega)=\frac{e^2\hat{c}_0}{ck_B T}f_{i0}\frac{1}{1+i\omega\tau_i} . \tag{15}$$

The relaxation time τ_i,

$$\tau_i=\frac{ef_{i0}}{Ac}\frac{1}{1+e^{-eV_0/k_B T}}e^{(e\Phi_{b0}+\epsilon_\xi)/k_B T}=f_{i0}\tau_i' , \tag{16}$$

depends exponentially on the barrier height Φ_{b0} and changes by several orders of magnitude as the dc bias V_0 is increased.

Given the modulation of the external bias V and the interface charge Q_i, we can calculate the *time dependence of the barrier height* Φ_b. This has to be done self-consistently as $\tilde{\Phi}_b$ shows up in Eq. (14) for $\tilde{Q}_i$. We relate the barrier modulation $\tilde{\Phi}_b$ to the variation in screening charge $Q_{l0}=eN_0x_{l0}$ and $Q_{r0}=eN_0x_{r0}$ by expansion of Eq. (2),

$$-\tilde{\Phi}_b=\frac{\tilde{Q}_{l0}}{C_l}=\frac{\tilde{Q}_{r0}}{C_r}-\tilde{V} , \tag{17}$$

where we have introduced the capacitance $C_l=\epsilon_0\epsilon/x_{l00}$ ($C_r=\epsilon_0\epsilon/x_{r00}$) of the left- (right-) hand-side depletion region. All charge variations, $\tilde{Q}_i$, $\tilde{Q}_{l0}$, and $\tilde{Q}_{r0}$, can now be expressed as a function of $\tilde{\Phi}_b$ and $\tilde{V}$, and with the neutrality condition

$$Q_i(t)=Q_{l0}(t)+Q_{r0}(t) ,$$

we can relate these two quantities to one another:

$$\tilde{\Phi}_b=\frac{C_r+C_i(\omega)/(1+e^{eV_0/k_B T})}{C_r+C_l+C_i(\omega)}\tilde{V} . \tag{18}$$

The time dependence of the barrier geometry is now completely determined.

The effects of the variations of the barrier can be detected in the external current. The dc part of this current is still well described by Eq. (11) with j and $\hat{c}$ substituted by their steady-state expressions j_0 and $\hat{c}_0$.

The ac *small-signal current* is made up of two contributions, a part flowing over the barrier and a displacement current $j_{ld}=-\dot{Q}_{l0}$ due to the time dependence of the screening charge Q_{l0}. The *over-barrier* part is found by expansion of Eq. (10):

$$\tilde{j}_{lb}=\sigma_0[(1-e^{-eV_0/k_BT})\tilde{\Phi}_b+e^{-eV_0/k_BT}\tilde{V}]$$
$$+\sigma_i(\omega)\left[\tilde{\Phi}_b-\frac{\tilde{V}}{1+e^{eV_0/k_BT}}\right] . \quad (19)$$

Here σ_0 is the zero-bias dc conductance

$$\sigma_0=j_0\frac{e}{k_BT}\left[1-\frac{\hat{c}_0}{2}\right] ,$$

and $\sigma_i(\omega)$ is a correction due to the trapping and emission by the interface,

$$\sigma_i(\omega)=j_0\frac{c}{2e}C_i(\omega)[(1+i\omega\tau_i')-e^{-eV_0/k_BT}(1-i\omega\tau_i')] .$$

The *displacement current* $j_{ld}=-\dot{Q}_{l0}$ is given by Eq. (17),

$$j_{ld}=i\omega C_l\tilde{\Phi}_b e^{i\omega t} .$$

The ac small-signal current finally is

$$j_{\text{ac}}=\sigma\tilde{V}e^{i\omega t}$$

with the *admittance* σ,

$$\sigma=[(1-e^{-eV_0/k_BT})\sigma_0+\sigma_i(\omega)+i\omega C_l]$$
$$\times\frac{C_r+C_i(\omega)/(1+e^{eV_0/k_BT})}{C_r+C_l+C_i(\omega)}$$
$$+\left[e^{-eV_0/k_BT}\sigma_0-\frac{\sigma_i(\omega)}{1+e^{eV_0/k_BT}}\right] . \quad (20)$$

This is our main result of this section.

The *zero-bias limit* of the admittance (20) is especially simple since (18) reduces to $\tilde{\Phi}_b/\tilde{V}=\frac{1}{2}$. The conductance G, defined as the real part of σ, becomes

$$G(\omega,V_0=0)=\text{Re}\sigma=\sigma_0 .$$

The capacitance C, which is proportional to the imaginary part of σ, is given by the high-frequency capacitance C_{HF} alone,

$$C(\omega,V_0=0)=\frac{1}{\omega}\text{Im}\sigma=\frac{\epsilon_0\epsilon}{x_{l00}+x_{r00}}=C_{\text{HF}} .$$

Thus the zero-bias limit of the admittance does not show any dispersion within this restricted model, which does not contain the deep bulk traps. This result is acceptable only for those situations where deep trap effects are of minor importance.[11] However, certain polycrystalline materials as, e.g., ZnO, can show a zero-bias dispersion in G ranging over several orders of magnitude.[18] Therefore it is imperative to take deep trap effects into account in a description of these materials. For $eV_0 \gg k_BT$ the result (20) also simplifies considerably.

B. Continuous DOS—localized states

We assume that the continuous DOS is made up of a homogeneous spatial distribution of single levels with different binding energies E_i. The matrix element for hopping between these states is taken to be zero (localized states) such that the interface is in thermal (quasi)equilibrium only by exchange with the bulk. No equilibration among the interface states is allowed. Thus each level acts independently of all others. Then we simply have to integrate the contributions from all single levels with their weight $N_i(E)$. The total interface charge variation $\tilde{Q}_i$ becomes

$$\tilde{Q}_i=e^2\int_{\xi_i^n}^{\infty}dE\,N_i(E)\frac{f_{i0}(E)[1-f_{i0}(E)]}{k_BT}$$
$$\times\frac{1}{1+i\omega\tau_i' f_{i0}(E)}\left[\tilde{\Phi}_b-\frac{\tilde{V}}{1+e^{eV_0/k_BT}}\right]$$
$$\cong e^2N_i(\xi_{i0})\int_0^1 df_{i0}\frac{1}{1+i\omega\tau_i' f_{i0}}\left[\tilde{\Phi}_b-\frac{\tilde{V}}{1+e^{eV_0/k_BT}}\right]$$
$$=C_i^l(\omega)\left[\tilde{\Phi}_b-\frac{\tilde{V}}{1+e^{eV_0/k_BT}}\right] ,$$

with the new interface capacitance $C_i^l(\omega)$ given by

$$C_i^l(\omega)=e^2N_i(\xi_{i0})\frac{\ln(1+i\omega\tau_i')}{i\omega\tau_i'} . \quad (21)$$

Here we assume that the DOS $N_i(E)$ is a smoothly varying function on the scale k_BT.

Note that the occupation statistics of the interface deviates from a Fermi distribution in this model as the quasi-Fermi-level ξ_i is energy dependent,

$$\tilde{\xi}_i(E)=\frac{1}{1+i\omega\tau_i(E)}\left[e\tilde{\Phi}_b-\frac{e\tilde{V}}{1+e^{eV_0/k_BT}}\right] .$$

The small-signal admittance σ is given by Eq. (20) with the new interface capacitance $C_i^l(\omega)$ and the integrated trapping probability $\hat{c}_0$, Eq. (12).

C. Continuous DOS—relaxed interface

We consider the case where the occupation statistics of the interface is always described by a Fermi function, i.e., the interface is in a (quasi)equilibrium at any moment. Such a thermal equilibrium is reached if the corresponding relaxation time is much smaller than $1/\nu$, where ν is the frequency of the applied field. The electrons are free to move between the different interface states in this model.

The dynamics for the interface charge Q_i is again given by an expression similar to Eq. (14), but with the capacitance now changed to[13]

$$C_i^r(\omega)=\frac{e^2\hat{c}_0}{2ck_BT}\frac{1}{1+i\omega\tau_i^r}$$

with the relaxation time

$$\tau_i^r=\frac{e}{2Ac}\frac{1}{1+e^{-eV_0/k_BT}}e^{(e\Phi_{b0}+\epsilon_\xi)/k_BT} .$$

Obviously we obtain these new expressions for $C_i^r(\omega)$ and τ_i^r out of the single-level formulas [Eqs. (15) and (16)] by substituting the value at the Fermi level $f_{i0}(\xi_{i0})=\frac{1}{2}$ for the occupation probability $f_{i0}(E_i)$. Similarly τ_i' is now defined as $2\tau_i^r$ and by taking the integrated trapping probability $\hat{c}_0$, all the necessary modifications to the single-level results are done.

The above discussion shows that our expression for the admittance σ, Eq. (20), is of a very general form, as it describes equally well the physical situation for different interface models. The only nontrivial changes are restricted to the interface capacitance.

The same is true for different models of the depletion region as described in Sec. IV (inclusion of deep trap effects): There, the additional modifications are restricted to the capacitances C_l and C_r of the depletion regions.

We close this section with an illustration of the differences in the small-signal response of the three interface models. In Figs. 6 and 7 we show the capacitance C as a function of dc bias V_0 and frequency ω. The case of a single interface level is compared to a Gaussian density of states using the localized model in one case and the relaxed model in the other.

The capacitance $C(V_0)$, shown in Fig. 6, changes from the high-frequency value C_{HF} at zero bias to a maximum which is about 1 order of magnitude larger. This increase is due to the resonant response of the interface: At higher bias V_0, the decaying barrier height Φ_b reduces the relaxation time τ_i [see Eq. (16)]. As soon as $\omega\tau_i(V_0) \lesssim 1$ the interface can follow the applied ac signal and the delayed filling and emptying of its states increases the capacitance. Finally, when the interface is filled, the states do not empty any more and the capacitance decays again to its high-frequency value. If the density of available states remains finite the decay of the capacitance to its high-frequency limit at high dc bias V_0 is inhibited.

The two different interface models for the continuous density of states give only minor differences in the shape of the resonance in $C(V_0)$. More drastic effects are found when the interface DOS is changed as, e.g., by concentrating this DOS symmetrically in a single level. The resulting modifications of the barrier $\Phi_b(V_0)$ (see Fig. 2) lead to a strong reduction in the capacitance resonance at the chosen frequency.

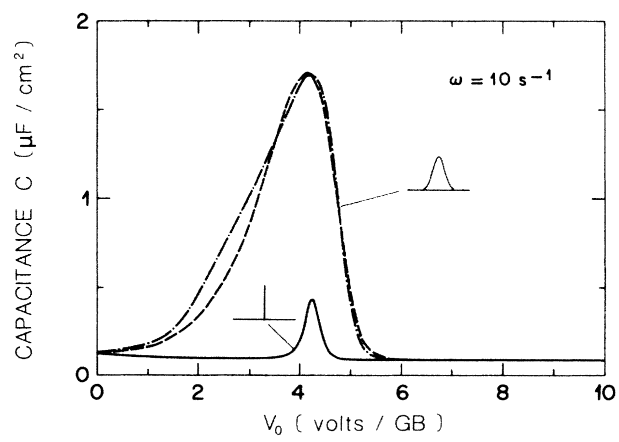

FIG. 6. Capacitance C versus applied dc bias V_0 for a single level and a Gaussian DOS for the interface. The localized states (— — —, Sec. III B) are compared to the relaxing model (—·—·—·, Sec. III C). No bulk traps are considered.

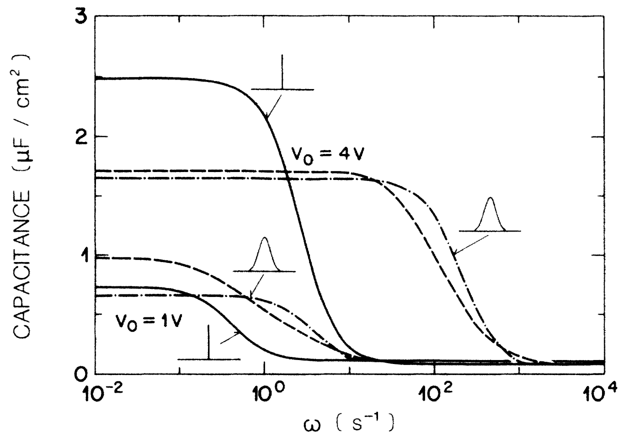

FIG. 7. Capacitance C versus frequency ω for dc bias $V_0 = 1$ and 4 V. The same interface models are used as in Fig. 6: ——, single level; — — —, localized; —·—·—·, relaxed,

The details of the frequency dependence are illustrated in Fig. 7 for two values of bias V_0. A general feature is the decay of the large low-frequency capacitance ($\omega\tau_i \lesssim 1$) to the high-frequency value C_{HF} when the interface states can no longer follow the ac signal. The decay is broader for the model with localized interface states. This is a consequence of the integration over the interface relaxation times which leads to a logarithmic behavior for $C_i^l(\omega)$ [Eq. (21)].

Next we discuss the situation for small frequencies ($eV_0 \gg k_B T$). A closer examination of Eq. (20) shows that the term proportional to σ_0 is responsible for the low-frequency capacitance, while the part due to the displacement current ($\propto i\omega C_l$) determines the high-frequency behavior. The low-frequency capacitance is then proportional to the ratio $\tilde{\Phi}_b/\tilde{V}$, and therefore

$$C \sim \sigma_0 \frac{C_r C_i \tau_i}{(C_r + C_l + C_i)^2}, \quad \omega \to 0$$

where C_i is the dc limit of the interface capacitance. For intermediate dc bias V_0 (interface states not completely filled), the interface capacitance is dominant ($C_r, C_l \ll C_i$); therefore, $C \sim 1/C_i$. The physical meaning of this situation is the following: The oscillations in screening charge ($\sim C_r \tilde{V}$) and interface charge ($C_i \tilde{\Phi}_b$) are equal by charge neutrality and, as the modulated over-barrier current dominates the net capacitance C at low frequencies, we obtain a large capacitance whenever $\tilde{\Phi}_b$ is large. This leads to the unexpected result that the capacitance C is large when the interface capacitance C_i is small.

As the interface states are filled, C_i decreases and the capacitances of the depletion regions, C_l and C_r, become dominant. The grain-boundary capacitance then decays to the high-frequency value C_{HF}.

Figure 7 shows again that the different interface models introduce only small changes in the response of the grain boundary. A major change in the capacitance is found for the limit of a single interface level. There a modified barrier geometry strongly affects the relaxation time τ_i, and hence the resonances are shifted to lower frequencies.

IV. TIME-DEPENDENT PROPERTIES INCLUDING DEEP BULK TRAPS

The inclusion of deep bulk traps introduces a new type of screening charge into our model. This screening charge differs from that due to the ionized shallow donors because of the finite response time of the deep states. Therefore new resonance effects can be expected in the small-signal response of the grain boundary.

We start again with the determination of the time-dependent geometry of the barrier. The result is then used to obtain the expression for the over-barrier current which now contains relaxation effects from the delayed response of the interface *and* the deep bulk traps. The total external current finally will pick up an additional contribution from the displacement currents generated by each deep trap.

For the study of the *dynamics of the deep bulk traps* we define the screening charges,

$$Q_{l\nu}=\int_{-\infty}^{0} Q_\nu(x)dx \quad \text{and} \quad Q_{r\nu}=\int_{0}^{\infty} Q_\nu(x)dx \ ,$$

with the screening charge densities $Q_\nu(x)$ given by[23(a)]

$$Q_\nu(x)=eN_\nu[1-f_\nu(x)], \quad \nu=1,\ldots,n \ .$$

The occupation number for the trap ν depends on position x and is given by the Fermi function

$$f_\nu(x)=\frac{1}{1+g_\nu e^{[E_\nu(x)-\xi(x)]/k_BT}} \ .$$

Here g_ν is the inverse of the degeneracy of the trap which can only be singly occupied (usually $g_\nu=\frac{1}{2}$). $E_\nu(x)$ and $\xi(x)$ are the position-dependent energies of the deep level and the Fermi level, respectively (see Fig. 1).

The response of the screening charge density under a change of applied bias is again limited by the amount of charge which is able to flow into or out of the traps. The equation of continuity then determines the rates,

$$\frac{d}{dt}Q_\nu(x,t)=-Ac_\nu N_\nu[1-f_\nu(x,t)]e^{-[E_c(x)-\xi]/k_BT} + b_\nu N_\nu f_\nu(x,t)e^{-\epsilon_\nu/k_BT} \ . \quad (22)$$

The first term on the right describes the trapping of electrons by the ionized states and the second the emission out of the occupied, neutral level. The capture cross section and the charge emission rate are again denoted by c_ν and b_ν, respectively, and their values are related to one another by $b_\nu=g_\nu Ac_\nu$ through the detailed balance condition for $\tilde{V}=0$.

The small-signal expansion of Eq. (22) relates the variation in screening charge density to the barrier geometry,

$$\tilde{Q}_\nu(x)=\frac{f_{\nu0}(x)[1-f_{\nu0}(x)]}{k_BT}\frac{eN_\nu}{1+i\omega\tau_\nu(x)}e\tilde{\Phi}(x) \ , \quad (23)$$

with the relaxation time

$$\tau_\nu(x)=\frac{e}{Ac_\nu}f_{\nu0}(x)e^{[E_{c0}(x)-\xi]/k_BT} \ .$$

We concentrate here on the traps to the left of the grain boundary. The calculation for the traps to the right proceeds along the same lines. However, the potential variation $\tilde{\Phi}(x)$ has to be substituted by $\tilde{\Phi}(x)+\tilde{V}$ since the relevant quantity is the variation of $E_c(x)$ with respect to the bulk Fermi level.

The product $f_{\nu0}(x)[1-f_{\nu0}(x)]/k_BT$ in Eq. (23) is a sharply peaked function at $E_{\nu0}(x)=\xi(x)$ (proportional to the derivative of the Fermi function). In general, we can approximate this expression by a δ function and then compare the result to the Schottky approximation for $\tilde{Q}_{l\nu}(x)$,

$$\tilde{Q}_{l\nu}(x)=\tilde{Q}_{l\nu}\delta(x+x_{l\nu0}) \ ,$$

$$\tilde{Q}_{l\nu}=\frac{eN_\nu}{|\Phi_0'(-x_{l\nu0})|}\frac{1}{1+i\omega\tau_\nu(-x_{l\nu0})}\tilde{\Phi}(-x_{l\nu0}) \ .$$

The potential variation $\tilde{\Phi}(-x_{l\nu0})$ can be expressed in terms of the screening charge amplitudes $\tilde{Q}_{l\mu}$ with $\mu<\nu$,

$$\frac{\tilde{\Phi}(-x_{l\nu0})}{|\Phi_0'(-x_{l\nu0})|}=\frac{\sum_{\mu=0}^{\nu-1}(x_{l\mu0}-x_{l\nu0})\tilde{Q}_{l\mu}}{\sum_{\mu=0}^{\nu-1}eN_\mu(x_{l\mu0}-x_{l\nu0})} \ .$$

With the definition

$$\tilde{Q}_{l\nu}=r_\nu\tilde{Q}_{l0} \ ,$$

we can relate the delayed dynamics of the deep trap screening charges to the instantaneous response of the shallow donor states. The coefficients r_ν are defined iteratively,[29]

$$r_\nu=\frac{1}{1+i\omega\tau_\nu}\frac{\sum_{\mu=0}^{\nu-1}(x_{l\mu0}-x_{l\nu0})r_\mu}{\sum_{\mu=0}^{\nu-1}(x_{l\mu0}-x_{l\nu0})(N_\mu/N_\nu)}, \quad r_0=1$$

$$\tau_\nu=\frac{e}{Ac_\nu(1+g_\nu)}e^{\epsilon_\nu/k_BT} \ .$$

We now express all charge variations as functions of $\tilde{\Phi}_b$ and $\tilde{V}$ [see Eq. (17)],

$$-\tilde{\Phi}_b=\left[\sum_{\nu=0}^{n}\frac{x_{l\nu0}}{\epsilon_0\epsilon}r_\nu\right]\tilde{Q}_{l0} = \left[\sum_{\nu=0}^{n}\frac{x_{r\nu0}}{\epsilon_0\epsilon}r_\nu\right]\tilde{Q}_{r0}-\tilde{V} \ ,$$

and use the neutrality condition

$$Q_i(t)=\sum_{\nu=0}^{n}[Q_{l\nu}(t)+Q_{r\nu}(t)]$$

to relate $\tilde{\Phi}_b$ to $\tilde{V}$. The result is identical to Eq. (18) but with the capacitances of the depletion regions now changed to

$$C_l=\epsilon_0\epsilon\frac{\sum_{\nu=0}^{n} r_\nu}{\sum_{\nu=0}^{n} x_{l\nu 0} r_\nu} \quad \text{and} \quad C_r=\epsilon_0\epsilon\frac{\sum_{\nu=0}^{n} r_\nu}{\sum_{\nu=0}^{n} x_{r\nu 0} r_\nu} . \tag{24}$$

In the above derivation the dynamics of the deep trap states is handled separately from the interface states. The capacitances C_l and C_r become mixed with the results for the interface capacitance (Sec. III) only in the calculation of the barrier geometry [Eq. (18)].

The above derivation has to be extended to include the situation where a deep trap, say $\nu=\lambda$, disappears below the quasi-Fermi-level. Here we assume that the quasi-Fermi-level is parallel to the conduction band at the boundary of the positive-biased grain (see Fig. 1). Such a spatial variation has been found for a diffusion-limited current flow by Pike.[25(b)] Whereas the screening charge $Q_{l\lambda}$ disappears smoothly as $e\Phi_b \rightarrow \epsilon'_\lambda$ ($x_{l\lambda}>0$), the charge $Q_{r\lambda}$ ($x_{r\lambda}>0$) is neutralized suddenly as the deep trap level crosses the quasi-Fermi-level. For *steady-state* properties this charge extinction can be described by a density renormalization,

$$N_\lambda \rightarrow N_\lambda(1-f_\lambda) ,$$

$$f_\lambda=f_\lambda(0)\cong\frac{1}{1+g_\lambda e^{(e\Phi_b-\epsilon'_\lambda)/k_BT}} .$$

The *dynamics* of the disappearing deep trap has to be treated separately. The product $f_{\lambda 0}(x)[1-f_{\lambda 0}(x)]$ in Eq. (23) cannot be approximated by a δ function. For the Fermi level running parallel to the deep trap level $E_{\lambda 0}(x)$, however, this product simplifies to the constant $f_\lambda(1-f_\lambda)$. Physically this means that not only the boundary layer of the charge $Q_{r\lambda}$ but the whole charge $Q_{r\lambda}$ responds to the applied small signal, thereby leading to a large capacitance. The dynamics of this charge is again given by Eq. (22) with the exponent $E_c(x)-\xi$ substituted by $E_c(0)-\xi$, as the trapped electrons originate predominantly from the left-hand side of the barrier. Integration over x leads to the result

$$\widetilde{Q}_{r\lambda}=-C^e_{r\lambda}\widetilde{\Phi}_b ,$$

with

$$C^e_{r\lambda}=e^2N_\lambda x_{r\lambda 0}\frac{f_\lambda(1-f_\lambda)}{k_BT}\frac{1}{1+i\omega\tau_\lambda} .$$

This additional charge modulation finally modifies the response of the barrier $\widetilde{\Phi}_b$ and Eq. (18) changes to

$$\widetilde{\Phi}_b=\frac{C_r+C_i(\omega)/(1+e^{eV_0/k_BT})}{C_r+C^e_r+C_l+C_i(\omega)}\widetilde{V} ,$$

with

$$C^e_r=\sum_{\nu=1}^{n} C^e_{r\nu}\frac{\sum_{\mu=0}^{n}(2x_{r\mu 0}-x_{r\nu 0})r_\mu}{2\sum_{\mu=0}^{n} x_{r\mu 0}r_\mu}$$

and with C_r and C_l still given by Eq. (24). Note that C^e_r is large only when a deep trap disappears below the Fermi level and can be neglected otherwise, thereby restoring the old result, Eq. (18).

The *over-barrier current* j_{lb} is entirely determined by the dynamics of the top of the barrier Φ_b [the term proportional to σ_0 in Eq. (19)] and the interface (σ_i). The result for $\widetilde{j}_{lb}$ of Sec. III therefore can also be used for the general case which includes the deep traps.

The *displacement current* j_{ld} is now the sum of all the contributions generated by the shallow and deep donor screening charges moving back and forth,

$$j_{ld}=-\sum_{\nu=0}^{n}\frac{d}{dt}Q_{l\nu}=i\omega C_l\widetilde{\Phi}_b e^{i\omega t} .$$

This is identical to the result of Sec. III but with the capacitance C_l now modified for the total screening charge according to Eq. (24).

Our main result for the *admittance* σ found in Sec. III, Eq. (20), proves now to be of a very general form. Different interface models are accounted for by choosing the appropriate formula for the interface capacitance $C_i(\omega)$, and the physics of the deep bulk traps is incorporated by adopting the suitable expressions for the depletion region capacitances C_l, C_r, and C^e_r.

A simple illustration of the general result is the *zero-bias limit* for the conductance G and the capacitance C. Again $\widetilde{\Phi}_b/\widetilde{V}=\frac{1}{2}$ due to the symmetry of the barrier. Taking into account only one deep trap level, we find

$$G(\omega,V_0=0)=\sigma_0+C_{\mathrm{HF}}\omega^2\frac{n_1\hat{\tau}_1}{1+(\omega\hat{\tau}_1)^2} ,$$

and

$$C(\omega,V_0=0)=C_{\mathrm{HF}}\left[1+\frac{n_1}{1+(\omega\hat{\tau}_1)^2}\right] ,$$

with

$$\hat{\tau}_1=\frac{\tau_1}{1+(N_1/N_0)(x_{l10}/x_{l00})}$$

and

$$n_1=\frac{N_1}{N_0}\frac{1-x_{l10}/x_{l00}}{1+(N_1/N_0)(x_{l10}/x_{l00})} .$$

For more than one defect state, the zero-bias capacitance and conductance are still described by a sum of simple Debye terms. However, a coupling among the individual traps is introduced by the relaxation coefficients r_ν. This coupling is weak for the situation where the shallow donor is the dominating trap, $N_\nu \ll N_0$, $\nu\geq 1$.

The presence of the deep bulk traps leads to a *zero-bias dispersion* in conductance and capacitance.[30] In the conductance G the dispersive term is weighted by a factor ω^2. Thus the deep trap resonances are best studied by analyzing G. On the other hand, for moderate bias V_0 the capacitance depends strongly on the relaxation properties of the interface as we will illustrate below. Therefore the effects due to the deep bulk traps and the interface states can be well distinguished and separately analyzed through a study of $G(\omega,V,T)$ and $C(\omega,V,T)$, respectively.

We conclude this section with an illustration of the admittance for a grain boundary characterized by three deep bulk traps of moderate density [case (a) in Table I] and a Gaussian DOS for the interface (localized model). In Fig. 8(a) we show the capacitance as a function of bias V_0 with frequency ω as a parameter. At moderate frequencies the curves are characterized by four well-separated resonances. The first, at lower bias values, is due to the interface as already discussed in Sec. III (Fig. 6). The three peaks at 4.5, 6.0, and 7.6 V indicate the neutralization of the deep traps as they disappear below the Fermi level. With the Fermi level parallel to the deep trap level, a lot of charge is dynamically captured and released at these bias values, leading to large peaks in the capacitance. As all deep traps are neutralized at high bias V_0 the capacitance returns to its high-frequency value C_{HF}.

The interface resonance at moderate bias shows a strong dispersion. The interface relaxation time τ_i decreases with increasing bias V_0. Therefore the resonance shifts to higher bias values with increasing ω. For $\omega \gtrsim 10^3$ s^{-1} the relaxation time $\tau_i < 10^{-3}$ s is reached only when all the interface states are already filled and the resonance has disappeared.

The deep trap resonances show no dispersion for $\omega \lesssim 10^3$ s^{-1} as their relaxation times are all small enough to give a full dynamic behavior at this temperature (see Table I). For $\omega \gtrsim 10^4$ s^{-1} the deep trap resonances are reduced as the trapping and emission of charge cannot follow the external signal any more.

In Fig. 8(b) the capacitance is plotted as a function of frequency ω for different values of V_0. The resonances for bias values $V_0 \leq 3$ V and $V_0 = 3.5$ V are assigned to the interface and the deepest bulk trap, respectively. The inset shows the deep trap resonances on an expanded scale. Their position does not depend on applied bias.

Figure 8(c) then illustrates the dependence of the capacitance C on temperature T. At low temperatures the interface is static because of the large relaxation time τ_i. This relaxation time shrinks with increasing T and for $\omega\tau_i(T) \lesssim 1$ the capacitance is enhanced by the dynamic interface. On an expanded scale we illustrate the freezing out of the deep trap states.

In Fig. 9(a) the conductance is reproduced as a function of applied bias V_0 with ω as a parameter. For small bias the small-signal conductance consists of a mixture of over-barrier (σ_0) and displacement current ($i\omega C_l$) with an increasing weight for the latter as ω is increased. As the bias V_0 is increased, Φ_b is reduced, and the over-barrier current takes over. In Fig. 9(b) we show the conductance as a function of frequency ω for several values of V_0. The (bias-independent) deep trap resonances are a pronounced feature of these curves. They indicate the onset of a displacement current as $\omega\tau_\nu \gtrsim 1$ for $\nu = 1, \ldots, 3$. The conductance is dominated by the barrier at low frequencies (strong dependence on V_0). At high frequencies the displacement currents dominate the leakage. Finally, Fig. 9(c) reproduces the conductance G as a function of temperature. This plot is most suited for a determination of the density, cross section, and energy position of the deep

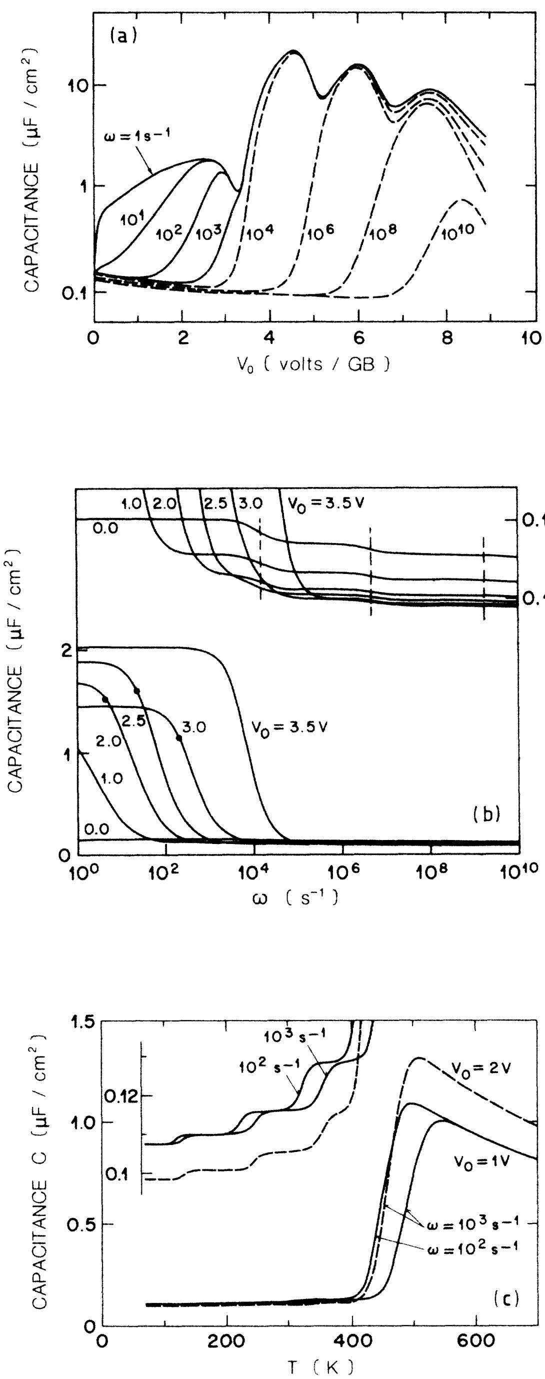

FIG. 8. (a) Capacitance C versus bias V_0 in the presence of deep bulk traps for a Gaussian DOS [Table I, case (a), localized model]. The curves are split into two classes, $\omega \lesssim 10^3$ s^{-1} and $\omega \gtrsim 10^4$ s^{-1}, as the interface and bulk trap relaxation time lie on different time scales: $\tau_i(V_0) \geq 10^{-3}$ s and $\tau_\nu \leq 10^{-4}$ s, $\nu = 1, \ldots, 3$. (b) Capacitance C versus frequency ω. At zero bias (and $V_0 = 3.5$ V) there is no interface contribution to the capacitance. The resonance for $V_0 = 3.5$ V is generated by the deepest trap ($\omega_{res} = 1.2 \times 10^4$ s^{-1}). The upper part shows the deep trap resonances on an enlarged scale. (c) Capacitance C versus temperature T. The dependence on bias for a fixed frequency and the frequency dependence for a fixed bias are illustrated.

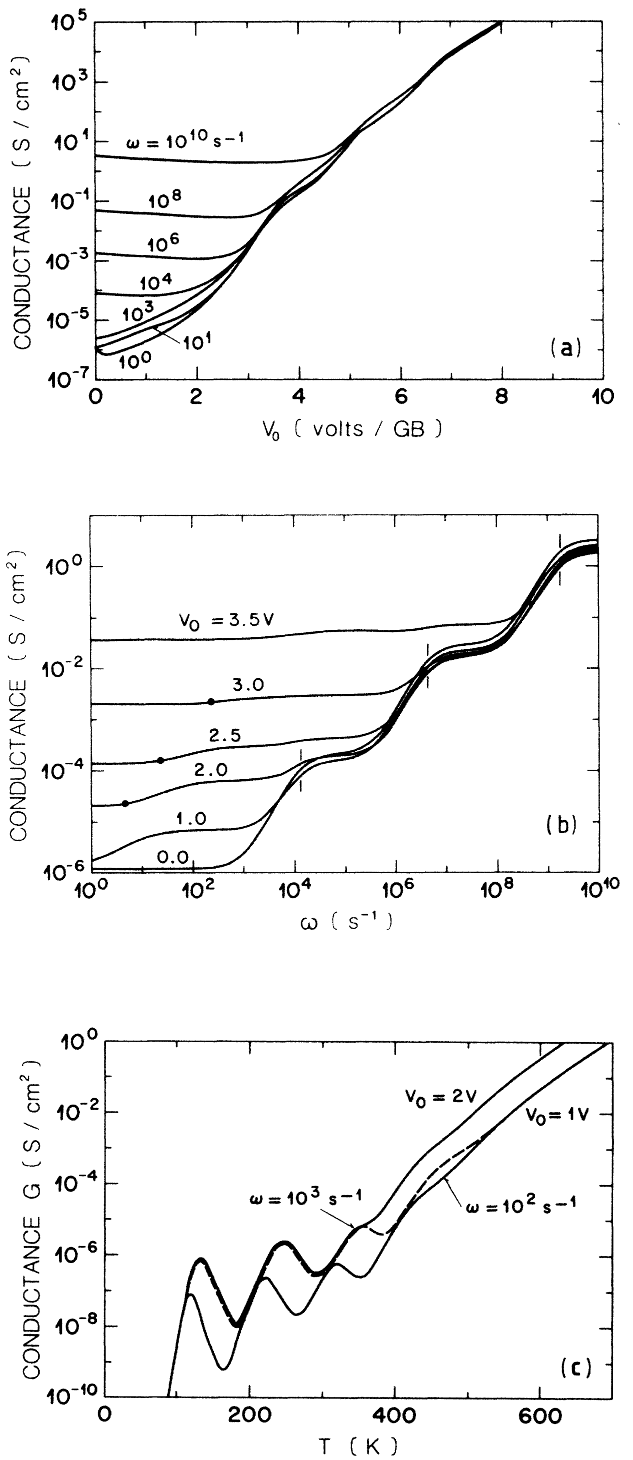

FIG. 9. (a) Conductance G versus bias V_0 for the grain-boundary parameters of Fig. 8(a). The large zero-bias dispersion is a relaxation effect of the bulk traps. The decaying barrier Φ_b leads to the exponential rise of G at large bias V_0. (b) Conductance G versus frequency ω. The position of the interface resonance depends on bias, whereas those for the deep traps do not. The grain boundary becomes transparent for the displacement currents at high frequencies. (c) Conductance G versus temperature T. The deep traps show pronounced frequency-dependent resonances at lower temperatures. For $T \gtrsim 400$ K the interface dominates ($V_0 > 0$).

trap levels.[18] At low temperature all relaxation effects are frozen in. With increasing T the relaxation times decay and each deep level develops its resonance as soon as $\omega\tau_\nu$ passes through 1, beginning with the fastest level (smallest ϵ_ν). At high enough temperatures also the interface is active for $V_0 > 0$. However, this resonance is hidden in the exponential rise of the conductance resulting from the increase of σ_0.

V. CONCLUSION

We have calculated the steady state and ac small-signal properties for majority carrier transport through a grain boundary. The transport properties are governed by the double Schottky-type potential barrier forming at the boundary as electrons are trapped in the interface states. The shape and position of the interface DOS determines to a major part the stability of the barrier when the applied voltage is increased. A second contribution to the stability, however, comes from the density of deep bulk traps. For donor states these additional levels tend to screen the interface charge more efficiently and thereby lower the potential barrier. The resulting current-voltage characteristic then shows a larger leakage and a smaller nonlinearity coefficient α. The inclusion of bulk defects into the description of grain boundaries is important for many practical situations, in particular when compound semiconductors are considered.[18]

The time-dependent properties of the grain boundary are strongly modified by the finite response time of the deep states at the interface and in the bulk. At moderate frequencies and bias the small-signal capacitance is strongly enhanced by the charge trapping at the interface while at high frequencies the conductance is magnified by several orders of magnitude as a consequence of the displacement currents generated through the dynamics of the deep bulk traps.

At large bias, when the interface states are almost filled, the bulk defects start to enhance the capacitance by inducing oscillations in the barrier height and hence in the over-barrier current. For practical situations, however, these effects occur at rather large current densities, where the experiments are difficult to perform.

We have discussed the effects of different shapes for the interface DOS on the steady-state properties (barrier stability, current transport, leakage, nonlinearity). Similarly, there is a strong dependence of the ac small-signal response on the form of the DOS. This has been shown by Pike[12] in a comparison for the two cases of a single level and a uniform distribution of interface states.

At present the question of the relaxation mechanism for the interface is rather unclear. Here two limits for the equilibration properties were considered: whereas the states are assumed to be strongly localized in the first case, the electrons are allowed to travel freely within the interface in the other limit (extended states). We found that the effects on the ac properties are small (besides a broadening of the capacitance resonance as a function of frequency for the localized model) when compared to the large changes introduced by variations in the interface DOS.

The temperature dependence of the conductance and the capacitance ($V_0>0$) is specially suitable for the determination of the microscopic parameters of the grain boundary. By choosing the appropriate bias, frequency, and/or temperature ranges it is possible to clearly separate the bulk from the interface contributions.

ACKNOWLEDGMENTS

The authors wish to thank C. Schüler and R. S. Perkins for their continuing interest and support. Many helpful discussions with J. Bernasconi, T. M. Rice, and G. E. Pike are gratefully acknowledged.

APPENDIX

We calculate the positions $x_{l\nu}$ and $x_{r\nu}$, $\nu=0,\ldots,n$ using the ansatz (2) for the potential $\Phi(x)$ and the conditions (3)—(5). Equation (3) leads to

$$2V=\sum_{\nu=0}^{n}\gamma_\nu(x_{r\nu}-x_{l\nu})(x_{r\nu}+x_{l\nu})\ ,$$

and (4) is used to find the relation

$$Q_i=\epsilon_0\epsilon\sum_{\nu=0}^{n}\gamma_\nu(x_{r\nu}+x_{l\nu})\ .$$

It is easy to see that $x_{r\nu}-x_{l\nu}=x_{r\mu}-x_{l\mu}$ for all pairings of ν and μ and therefore we can relate $x_{r\mu}$ to $x_{l\mu}$ by

$$x_{r\mu}=x_{l\mu}+2\epsilon_0\epsilon V/Q_i\ . \tag{A1}$$

Next we relate the positions $x_{l\nu}$, $\nu\geq1$, to the barrier boundary x_{l0}. We use Eqs. (2) and (5) to find

$$\sum_{\mu=0}^{\nu-1}e\gamma_\mu(x_{l\mu}-x_{l\nu})^2=2\epsilon'_\nu,\quad \nu\geq1\ . \tag{A2}$$

With the definition

$$(b_\nu)^{1/2}=x_{l0}-x_{l\nu}$$

we calculate the distance $(b_\nu)^{1/2}$ under the assumption that these quantities are known for $\mu<\nu$. Using (A2), we have to solve a quadratic equation for $(b_\nu)^{1/2}$,

$$\left[\sum_{0}^{\nu-1}\gamma_\mu\right]b_\nu-2\left[\sum_{1}^{\nu-1}\gamma_\mu(b_\mu)^{1/2}\right](b_\nu)^{1/2}+\left[\sum_{1}^{\nu-1}\gamma_\mu b_\mu-\frac{2\epsilon'_\nu}{e}\right]=0\ ,$$

and using the abbreviations of Sec. II we find the solution

$$(b_\nu)^{1/2}=\alpha_{\nu-1}+(\alpha_{\nu-1}^2-\beta_{\nu-1}+n_0^{\nu-1}a_\nu)^{1/2}\ , \tag{A3}$$

with

$$\beta_\nu=\sum_{\mu=1}^{\nu}n_\mu^\nu b_\mu\ .$$

For $\nu=1$ the result

$$(b_1)^{1/2}=n_0^0a_1=\frac{2}{\gamma_0e}\epsilon'_1 \tag{A4}$$

is found immediately, thus all distances $(b_\nu)^{1/2}$ are determined by (A3). Finally, we obtain the position of the barrier boundaries x_{l0} and x_{r0} by using again the neutrality condition, Eq. (4):

$$\frac{Q_i}{\epsilon_0\epsilon}=\sum_{\nu=0}^{n}\gamma_\nu(x_{l\nu}+x_{r\nu})$$

$$=(x_{l0}+x_{r0})\sum_{\nu=0}^{n}\gamma_\nu-2\sum_{\nu=1}^{n}\gamma_\nu(b_\nu)^{1/2}\ ,$$

and with (A1) we find

$$x_{l0}=\frac{1}{2\gamma}\left[\frac{Q_i}{\epsilon_0\epsilon}+2\sum_{\nu=1}^{n}\gamma_\nu(b_\nu)^{1/2}\right]-\frac{\epsilon_0\epsilon V}{Q_i}\ . \tag{A5}$$

Equations (A1), (A3), (A4), and (A5) now determine all $2(n+1)$ positions $x_{l\nu}$ and $x_{r\nu}$.

Note that there is a difference in the handling of shallow and deep states. The boundaries x_{l0} and x_{r0} are determined by the neutrality condition of the barrier, whereas the boundaries of the deep trap screening charges, $x_{l\nu}$ and $x_{r\nu}$, $\nu>0$, are given by Eq. (5), the condition for the crossover of the deep level and the bulk Fermi level. Therefore N_0 describes the density of *all* shallow levels, i.e., levels lying above the Fermi level. Their positions enter the calculation merely in the determination of the Fermi level, but not in the calculation of the barrier geometry. This is due to the fact that these states are assumed to be everywhere ionized and the neutralizing charge away from the barrier is given by the electrons in the conduction band.

The result (A3) can be simplified using the relation

$$\beta_\nu-\alpha_\nu^2=n_0^\nu\sum_{\mu=1}^{\nu}n_\mu^\nu a_\mu\ . \tag{A6}$$

We prove this by induction:

$$\beta_\nu-\alpha_\nu^2=\sum_{\mu=1}^{\nu}n_\mu^\nu b_\mu-\left[\sum_{\mu=1}^{\nu}n_\mu^\nu(b_\mu)^{1/2}\right]^2$$

$$=\beta_{\nu-1}+n_\nu^\nu b_\nu+\sum_{\mu=1}^{\nu-1}(n_\mu^\nu-n_\mu^{\nu-1})b_\mu-\left[\alpha_{\nu-1}+n_\nu^\nu(b_\nu)^{1/2}+\sum_{\mu=1}^{\nu-1}(n_\mu^\nu-n_\mu^{\nu-1})(b_\mu)^{1/2}\right]^2.$$

Using the identity

$$n_\mu^\nu-n_\mu^{\nu-1}=-n_\nu^\nu n_\mu^{\nu-1}\ ,$$

we obtain

$$\beta_\nu-\alpha_\nu^2=\beta_{\nu-1}+n_\nu^\nu(b_\nu-\beta_{\nu-1})-\{\alpha_{\nu-1}+n_\nu^\nu[(b_\nu)^{1/2}-\alpha_{\nu-1}]\}^2$$
$$=(1-n_\nu^\nu)(\beta_{\nu-1}-\alpha_{\nu-1}^2)+n_\nu^\nu(1-n_\nu^\nu)\{(b_\nu)^{1/2}[(b_\nu)^{1/2}-2\alpha_{\nu-1}]+\alpha_{\nu-1}^2\} .$$

Inserting the expression (A3) for $(b_\nu)^{1/2}$, we find

$$\beta_\nu-\alpha_\nu^2=(\beta_{\nu-1}-\alpha_{\nu-1}^2)(1-n_\nu^\nu)^2+n_\nu^\nu(1-n_\nu^\nu)n_0^{\nu-1}a_\nu .$$

Assuming now that Eq. (A6) is true for $\nu-1$ and using the relation

$$1-n_\nu^\nu=\frac{n_\lambda^\nu}{n_\lambda^{\nu-1}},\quad \lambda=0,\ldots,\nu$$

we obtain the desired result

$$\beta_\nu-\alpha_\nu^2=n_0^\nu\sum_{\mu=1}^{\nu}n_\mu^\nu a_\mu .$$

Finally, using $b_1=a_1$, it is easily shown that (A6) is true for $\nu=1$.

Equation (A6) is not only used for the simplification of (A3) but also for the determination of the barrier height Φ_b. Evaluation of Eq. (2) at $x=0$ gives

$$\Phi_b=\sum_{\nu=0}^{n}\frac{\gamma_\nu}{2}x_{l\nu}^2=\frac{\gamma_0}{2}x_{l0}^2+\sum_{\nu=1}^{n}\frac{\gamma_\nu}{2}[x_{l0}-(b_\nu)^{1/2}]^2$$
$$=\frac{\gamma}{2}x_{l0}^2-\gamma x_{l0}\alpha_n+\frac{\gamma}{2}\beta_n ,$$

and using the relation for x_{l0},

$$x_{l0}=\frac{1}{2\gamma}\left[\frac{Q_i}{\epsilon_0\epsilon}-\frac{\epsilon_0\epsilon V}{Q_i}\right]+\alpha_n ,$$

we find

$$\Phi_b=\tfrac{1}{4}V_c\left[1-\frac{V}{V_c}\right]^2+\frac{\gamma}{2}(\beta_n-\alpha_n^2) .$$

Inserting Eq. (A6) here immediately leads to the desired result, Eq. (6).

[1]For a recent review, see *Polycrystalline Semiconductors,* Vol. 57 of *Springer Series in Solid-State Sciences,* edited by G. Harbeke (Springer, Berlin, 1985).

[2]A. Bourret, in Ref. 1.

[3]R. E. Thomson and D. J. Chadi, Phys. Rev. B **29**, 889 (1984); H. J. Möller and H. H. Singer, in Ref. 1; D. P. DiVincenzo, Bull. Am. Phys. Soc. **30**, 536 (1985).

[4]J. Bernasconi, H. P. Klein, B. Knecht, and S. Strässler, J. Electron. Mater. **5**, 473 (1976); Solid State Commun. **21**, 867 (1977).

[5]L. M. Levinson and H. R. Philipp, J. Appl. Phys. **47**, 1117 (1976); **49**, 6142 (1978); G. D. Mahan, L. M. Levinson, and H. R. Philipp, *ibid.* **50**, 2799 (1979).

[6]G. E. Pike and C. H. Seager, J. Appl. Phys. **50**, 3414 (1979).

[7]C. H. Seager and G. E. Pike, Appl. Phys. Lett. **37**, 747 (1980); Phys. Lett. **40**, 471 (1982).

[8]M. G. Spencer, W. J. Schaff, and D. K. Wagner, J. Appl. Phys. **54**, 1429 (1983).

[9]G. C. McCognial, D. J. Thomson, J. G. Shaw, and H. C. Card, Phys. Rev. B **28**, 5908 (1983).

[10]H. F. Mataré, J. Appl. Phys. **56**, 2605 (1984).

[11]J. Werner and H. Strunk, J. Phys. C **1**, 89 (1982); J. Werner, Ph.D. thesis, University of Stuttgart, 1983; and in Ref. 1.

[12]G. E. Pike, Phys. Rev. B **30**, 795 (1984).

[13]G. Blatter and F. Greuter, in Ref. 1.

[14]D. V. Lang, J. Appl. Phys. **45**, 3023 (1974); A. Broniatowski, in Ref. 1.

[15]W. G. Oldham and S. S. Naik, Solid-State Electron. **15**, 1085 (1972).

[16]Y. Zohta, Solid-State Electron. **16**, 1029 (1973).

[17]D. L. Losee, J. Appl. Phys. **46**, 2204 (1975).

[18]F. Greuter and G. Blatter (unpublished).

[19]G. E. Pike, *Grain Boundaries in Semiconductors,* edited by H. J. Leamy *et al.* (North-Holland, Amsterdam, 1982), p. 369.

[20]F. Greuter, J. Bernasconi, and R. S. Perkins, Am. Ceram. Soc. Bull. **63**, 480 (1984), and unpublished work.

[21]G. E. Pike, S. R. Kurtz, P. L. Gourley, H. R. Philipp, and L. M. Levinson, J. Appl. Phys. **57**, 5512 (1985); Am. Ceram. Soc. Bull. **63**, 480 (1984).

[22]F. Greuter and E. Gisler, Europhys. Conf. Abstr. **9C**, 302 (1985), and unpublished.

[23](a) A deep acceptor is treated as a deep donor after subtraction of its density from the dominant shallow donor density N_0. (b) For simplicity we only consider acceptorlike interface states. The extension to donorlike states or any precharge is straightforward.

[24]We assume that the quasi-Fermi-level is parallel to the conduction-band edge for $0\le x\le x_{r\lambda}$; see also Fig. 1 and Ref. 25(b).

[25](a) R. K. Mueller, J. Appl. Phys. **32**, 635 (1961). The result applies to a thermionic emission model for the electron trasport, but a diffusion limited approach leads to a similar result, see Ref. 24. (b) G. E. Pike, Phys. Rev. B **30**, 3274 (1984).

[26]For a deep acceptor level an increase in density leads to a higher barrier, contrary to the case of a deep donor state. The first term in Eq. (6) remains unchanged and the second increases with the acceptor density.

[27]G. Blatter and F. Greuter (unpublished).

[28]We denote the steady-state part by a subscript 0 and the linear response amplitude by a tilde. Only $\tilde{\Phi}_b$ is defined with a

minus sign.

[29]The same coefficients r_ν also describe the relaxation of the screening charges on the right-hand side because of the equality $x_{r\mu 0}-x_{r\nu 0}=x_{l\mu 0}-x_{l\nu 0}$.

[30]A zero-bias dispersion in the small-signal admittance may also be obtained by an asymmetrically doped barrier without deep traps. The result [Eq. (20)] is still valid, however, $C_l \neq C_r$ already at zero bias and hence $\tilde{\Phi}_b/\tilde{V}$ depends on $C_i(\omega)$. This adds an additional resonance to the zero-bias response which is due to the finite relaxation time of the interface.